

# Formation of Cyanoformaldehyde in the interstellar space

A. Das<sup>1</sup>, L. Majumdar<sup>1</sup>, S. K. Chakrabarti<sup>1,2</sup>, R. Saha<sup>1</sup>, S. Chakrabarti<sup>1,3</sup>

<sup>1</sup>Indian Centre for Space Physics, Chalantika 43, Garia Station Rd., Kolkata 700084, India

<sup>2</sup>S. N. Bose National Centre for Basic Sciences, Salt Lake, Kolkata 700098, India

<sup>3</sup>Maharaja Manindra Chandra College, 20 Ramakanta Bose lane, Kolkata 700003, India

## ABSTRACT

Cyanoformaldehyde (HCOCN) molecule has recently been suspected towards the Sagittarius B2(N) by the Green Bank telescope, though a confirmation of this observation has not yet been made. In and around a star forming region, this molecule could be formed by the exothermic reaction between two abundant interstellar species, H<sub>2</sub>CO and CN. Till date, the reaction rate coefficient for the formation of this molecule is unknown. Educated guesses were used to explain the abundance of this molecule by chemical modeling. In this paper, we carried out quantum chemical calculations to find out empirical rate coefficients for the formation of HCOCN and different chemical properties during the formation of HCOCN molecules. Though HCOCN is stable against unimolecular decomposition, this gas phase molecule could be destroyed by many other means, like: ion-molecular reactions or by the effect of cosmic rays. Ion-molecular reaction rates are computed by using the capture theories. We have also included the obtained rate coefficients into our large gas-grain chemical network to study the chemical evolution of these species in various interstellar conditions. Formation of one of the isotopologue(DCOCN) of HCOCN is also studied. Our study predicts the possibility of finding HCOCN and DCOCN in the ice phase with a reasonably high abundance. In order to detect HCOCN or DCOCN in various interstellar environments, it is necessary to know the spectroscopic properties of these molecules. To this effect, we carried out quantum chemical calculations to find out different spectral parameters of HCOCN for the transition in electronic, infrared and rotational modes. We clearly show how the isotopic substitution (DCOCN) plays a part in the vibrational progressions of HCOCN.

**Key words:** Astrochemistry, spectra, ISM: molecules, ISM: abundances, ISM: evolution, methods: numerical

## 1 INTRODUCTION

Several complex molecules are found not only in the interstellar clouds but also in comets, planetary nebulae, stellar atmosphere, circumstellar envelopes etc. According to the Cologne Database for Molecular Spectroscopy (CDMS) catalog (Muller et al., (2001) & Muller et al., (2005)) approximately 170 molecules have been detected in the interstellar medium or circumstellar shells. These molecules play an active role in the energy balance of the clouds. Despite these overwhelmingly significant observational evidences, till date, chemical composition of the gas is not well resolved. Discovery of more than 20 interstellar molecules in the ice phase confirmed wide spread presence of the interstellar dust in and around ISM. Theoretical models (Chakrabarti et al., 2006ab; Das et al., 2008ab; Das, Acharyya& Chakrabarti 2010; Cuppen & Herbst 2007; Cuppen et al., 2009; Das & Chakrabarti 2011 etc.) indicated that these dusts play a major role for deciding the chemical composition in any molecular cloud. From the laboratory experiments and observational results, it is found that 90% of the grain mantle is covered with H<sub>2</sub>O, CH<sub>3</sub>OH and CO<sub>2</sub>. The chemical composition of the gas phase of any molecular cloud is heavily dictated by its environment. Both the gas and the grain chemistry are influenced by radiation coming from nearby young stars. Several studies related to the coupled hydro-chemical model are also present in the literature (e.g., Aikawa et al., 2005, Das et al., 2008a, Das et al., 2013). These studies explore the possibility of formation of several complex molecules in different regions of the molecular cloud.

**Table 1.** Initial abundances used relative to the total hydrogen nuclei.

Species	Abundance
H <sub>2</sub>	$5.00 \times 10^{-01}$
He	$1.00 \times 10^{-01}$
N	$2.14 \times 10^{-05}$
O	$1.76 \times 10^{-04}$
H <sub>3</sub> <sup>+</sup>	$1.00 \times 10^{-11}$
C <sup>+</sup>	$7.30 \times 10^{-05}$
S <sup>+</sup>	$8.00 \times 10^{-08}$
Si <sup>+</sup>	$8.00 \times 10^{-09}$
Fe <sup>+</sup>	$3.00 \times 10^{-09}$
Na <sup>+</sup>	$2.00 \times 10^{-09}$
Mg <sup>+</sup>	$7.00 \times 10^{-09}$
P <sup>+</sup>	$3.00 \times 10^{-09}$
Cl <sup>+</sup>	$4.00 \times 10^{-09}$
e <sup>-</sup>	$7.31 \times 10^{-05}$

Recently, Majumdar et al., (2013) performed a quantum chemical calculation to obtain the spectral signatures (infrared and electronic absorption spectra) of the precursors of some bio-molecules such as adenine, alanine and glycine. It was found that the spectral signature of the gas phase significantly differs from that in the ice phase. These type of theoretical results provide one with ideal tools for serving as the benchmark for the observations. Several unidentified bands (Unidentified Infrared emission, Allamandola, Hudgins & Sandford, 1999) were identified which could be due to the hydrocarbon families. So, observations of some species, which are closely related to the hydrocarbon chains could be important clues for modeling purpose (Gerin et al., 1989). Formaldehyde (H<sub>2</sub>CO) and HCOCN abundances could be strongly inter-related since they might have followed the same chemical history. In case of HCOCN, there is a substitution of an H atom by a CN radical. In this paper, we discuss different properties of HCOCN and one of its isotopologues, namely, DCOCN. The plan of this paper is the following: In Section 2, the models and the computational details are presented. Implications of the results are discussed in Section 3. Finally, in Section 4, we draw our conclusions. In Appendix A, we tabulate some of the spectral information in the format of JPL catalog.

## 2 COMPUTATIONAL DETAILS

### 2.1 Gas phase reaction rate coefficients

Density functional theory (DFT) is an efficient tool to explore the chemical parameters of a species. We use the DFT formalism explicitly to find out different chemical parameters for the synthesis of interstellar cyanoformaldehyde. Cyanoformaldehyde has an asymmetric top configuration with dipole moments along the two principal axes. It is composed of two functional groups (aldehyde and cyano). The computations were performed using Becke three-parameter Exchange and Lee, Yang and Parr correlation (B3LYP) functional (Becke, 1993) with the 6-311++G\*\* basis set available in the Gaussian 09W package. Total energies, zero point vibrational energies, electronic energies and activation barrier energies, of all the species, which are formed during the synthesis of HCOCN are calculated.

Rate coefficients for a chemical reaction could be calculated by using the conventional transition state theory. According to this theory, the rate coefficient has the following form:

$$k(T) = (K_B T / h C^0) \exp(-\Delta G / RT) \text{ s}^{-1}, \quad (1)$$

where  $K_B$  is the Boltzmann constant,  $h$  is the Planck's constant,  $T$  is the temperature,  $C^0$  is the concentration (set to 1, following Jalbout & Shipar, 2008),  $R$  is the ideal gas constant, and  $\Delta G$  is the free energy of activation. It is clear from the above equation that the rate constant is strongly dependent of temperature.

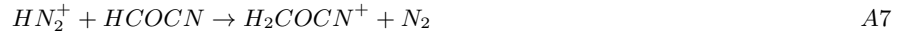
According to Remijan et al. (2008), gas phase Cyanoformaldehyde could be formed by the reaction of the cyanide (CN) radical and neutral formaldehyde (H<sub>2</sub>CO):



This type of reaction is often barrier less and exothermic in nature (Balucani et al., 2002). H<sub>2</sub>CO and CN are known to have wide-spread spatial distributions and relatively high abundances in the interstellar clouds (Zuckerman & Palmer, 1974; Churchwell, 1980). Earlier, it was believed that HCOCN is an unstable species that would quickly undergo unimolecular decomposition into products of HCN and CO (e.g., Judge et al. 1986; Clouthier & Moule 1987). Lewis-Bevan et al., (1992) showed that the decomposition energy for the HCOCN is much higher (68.74 Kcal mol<sup>-1</sup>  $\sim$  16, 700K). So once produced,

HCOCN could survive in the interstellar environment, when shielded from the general stellar and galactic radiation fields, i.e., in the dense cloud.

Though HCOCN is stable against unimolecular decomposition, this gas phase molecule could be destroyed by many other interstellar chemical processes such as; ion-molecular reactions or by the effect of cosmic rays. Since gas-phase chemistry of cold regions could be dominated by the exothermic ion-molecule reactions, these pathways could be served as a dominant destruction pathways for any gas phase neutral molecules. We have included these pathways into our gas phase chemical network for the destruction of gas phase HCOCN. First of all, from Woodall et al., (2007), we have selected the major ions in their gas phase chemical network (for this selection, steady state abundances of the ions are shortlisted and if the abundance of any ion is found to be greater than  $10^{-10}$  with respect to molecular hydrogen then it is selected). From Woodall et al., (2007), we found that abundances of  $C^+$ ,  $H_3O^+$ ,  $HCO^+$ ,  $H_3^+$ ,  $Na^+$ ,  $Mg^+$ ,  $Fe^+$ ,  $O_2^+$ ,  $HN_2^+$ ,  $NO^+$ ,  $HNO^+$  and  $H^+$  were beyond  $10^{-10}$  with respect to the molecular hydrogen. Now, gas phase HCOCN molecules are mainly producing by the reaction A1, where one H atom of the  $H_2CO$  molecule is substituted by a CN radical. Despite of this substitution, here we have assumed that HCOCN is interacting with the ions as the same way as  $H_2CO$  does. In between the shortlisted ions, we only have considered those ion-molecular destruction reaction for HCOCN molecule (from Woodall et al., 2007 network), for which the ion-molecular destruction pathways are available for the  $H_2CO$  molecule. Following are the list of ion-molecular reactions considered here for the destruction of gas phase HCOCN;



According to Herbst (1996), reaction rate coefficients for the reactions that do not possess a potential energy barrier at short-range, long-range capture theories could be applied. Such theories assume that all hard collisions lead to reaction and this collisions occur for all partial waves up to a maximum impact parameter or relative angular momentum quantum number. According to them, the centrifugal barrier produces a long-range maximum in the effective potential energy function ( $V_{eff}$ ):

$$V_{eff}(r, b) = v(r) + T_{AB}b^2/r^2,$$

where,  $r$  is the separation between the reactants and  $T_{AB}b^2/r^2$  is the angular kinetic energy. If the reactants could able to overcome the centrifugal barrier, they would spiral in towards each other in the absence of short-range repulsive forces. The long-range potential (in cgs-esu units) in this situation could be written as follows:

$$V(r) = e^2\alpha_d/2r^4,$$

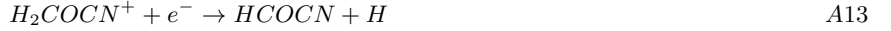
where  $\alpha_d$  is the polarizability of the neutral reactant. This potential leads to the Langevin rate coefficient

$$k = v\pi b_{max}^2 = 2\pi e\sqrt{\alpha_d/\mu} \quad (2)$$

where  $b_{max}$  is the maximum impact parameter,  $\mu$  is the reduced mass of the reactants. This theory predicts a temperature independent rate coefficient with magnitude  $\sim 10^{-9} cm^3 s^{-1}$ . Several experiments confirm the validity of this theory for the majority of ion-molecule reactions which appear rarely to possess potential energy surfaces with short range barriers. For the case of reaction (A2-A10), HCOCN is the neutral reactant and from our quantum chemical calculation, we get  $\alpha_d = 28.62$  Bohr<sup>3</sup> (1 Bohr = 0.529 Å<sup>3</sup>) for HCOCN. So from Eqn. 2, we could calculate the reaction rates for the ion-molecular reactions (A2-A10) by just plugging the reduced mass of the respective reactants.

Gas phase ions are mainly destroyed by the Dissociative Recombination (hereafter, DR) process. DR pathways for the destruction of all the ions which are producing during the ion-molecular reactions (A2-A10), are already into our network except  $H_2COCN^+$ . Here, we assume that  $H_2COCN^+$  has the similarity with  $H_3CO^+$  (one H atom of  $H_3CO^+$  could be substituted by a CN radical to form  $H_2COCN^+$ ). Following the DR pathways of the  $H_3CO^+$ , here we have considered the following dissociative recombination pathways with the similar rate coefficient for  $H_2COCN^+$ :





Interstellar species could be destroyed due the effect of cosmic rays even inside a dense cloud. According to Ding, Fang & Liu (2003), HCOCN could be photo-dissociated into following two channels:



Rate of above photo-reactions (A14 & A15) could be adopted as follows:

$$k_{CR}(T) = \alpha(T/300)^\beta \gamma / (1 - \omega), \quad (3)$$

where,  $\alpha$  is the cosmic-ray ionization rate,  $\gamma$  is the probability per cosmic-ray ionization that the appropriate photo reaction takes place, and  $\omega$  is the dust grain albedo in the far ultraviolet. Following, Woodall et al., (2007), we use the cosmic ray ionization rate  $\alpha = 1.30 \times 10^{-17}$  ionization per sec,  $\beta = 0$ ,  $\omega=0.6$ .  $\gamma$  is highly sensitive to the reactants and thus to start with an educated estimation, unless otherwise stated, we use  $\gamma = 1$  for the reactions A14 & A15. As we are considering the gas-grain interaction, some gas phase HCOCN could be accreted on the grain surfaces and thus could be depleted from the gas phase. This process is also a depletion mechanism for HCOCN as far as the gas chemistry is concerned.

According to Nguyen and Nguyen, (1999), HCOCN could also be destroyed by the following reactions:



The heat of formation for the above four reactions are 57.2 KJ/mol, 57.1 KJ/mol, 55.5 KJ/mol and 60.0 KJ/mol respectively (Nguyen and Nguyen, 1999). Now, in cold interstellar clouds, averaged translational temperatures of the reactants are about 10K, which can rise up to 4000K in the outer photosphere of carbon stars (Kaiser et al., 1999). Since 4000K is roughly equivalent to 40KJ/mol, all the four reactions (A16-A19) do not influence the destruction of HCOCN in the dense cloud.

In our quantum chemical modeling, B3LYP method and 6-311++G\*\* basis set are used for the calculation of the transition state for the above reactions. The results of the transition state calculations show that the reaction has a negative activation energy both in the gas ( $E_0 = -0.825499$  eV) as well as in the grain (water ice) phase ( $E_0 = -0.609866$  eV). Any elementary reactions exhibiting these negative activation energies are typically barrier-less in nature and the reactions rely on the capture of the molecules in a potential well. Reaction rate coefficient for such a reaction A1 could be calculated by using Eqn. 1. For the gas phase reaction A1, Quantum chemical calculation during the transition state provides,  $\Delta G$ . (Free energy of activation with the thermal correction) = 1.60381843 Kcal/mole. Here, we restrict our simulations in the temperature range of 10 – 20K, which is feasible for the dense cloud condition. It is clear from the rate expression (Eqn. 1) that it has an exponential dependency on the temperature. During this temperature range (10 – 20K), the gas phase Rate coefficients for reaction A1 varies from  $1.838 \times 10^{-24} s^{-1}$  to  $1.237 \times 10^{-06} s^{-1}$ .

## 2.2 Surface reaction rate coefficients

We have assumed that the gas phase species are physisorbed onto the dust grains ( $\sim 1000 \text{ \AA}$ ) having a grain number density of  $1.33 \times 10^{-12} n_H$ , where  $n_H$  is the concentration of H nuclei in all forms. Binding energies of the surface species are the keys for the chemical enrichment of the interstellar grain mantles. Grain surface provides the space for the interstellar gas phase species to land on and to react with other surface species. Chemical species can return back to the gas phase after chemical reactions or in the original accreted form. Reactions among the surface species are highly dependent on their mobility which in turn, depends on the thermal hopping time scale or on the tunneling time scale whichever is shorter. For the lighter species, the tunneling time scale is much shorter than the hopping time scale. When two surface species meet, they can react. If some activation energy is required for that reaction to happen, the reaction occur with a quantum mechanical tunneling probability. Following Hasegawa, Herbst & Leung (1992), reaction rate ( $R_{ab}$ ) between the surface species  $a$  and  $b$  can be expressed as;

$$R_{ab} = k_{ab}(R_{d,a} + R_{d,b})N_a N_b n_d, \quad (4)$$

where,  $N_a$  and  $N_b$  are the the number of species ‘a’ and ‘b’ on an average grain respectively,  $k_{ab}$  is the probability for the reaction to happen upon an encounter and  $n_d$  is the dust-grain number density,  $R_{d,a}$  and  $R_{d,b}$  are the diffusion rate respectively for the species ‘a’ and ‘b’. Diffusion rate ( $R_{d,a} = \frac{1}{N_S t_{d,a}}$ ) depends upon the time needed to traverse entire grain by the reactive species, which in turn depends on

$$t_{d,a} = \nu_0^{-1} \exp(E_b/kT_g) \text{sec}, \quad (5)$$

where,  $\nu_0$  is the characteristic vibration frequency of the adsorbed species,  $E_b$  is the potential energy barrier between adjacent surface potential energy wells,  $T_g$  is the grain temperature and  $N_S$  is the number of surface sites on a grain. For the computation of the characteristic vibration frequency ( $\nu_0$ ), we have utilized the following harmonic oscillator relation:

$$\nu_0 = \sqrt{(2n_s E_d / \pi^2 m)}, \quad (6)$$

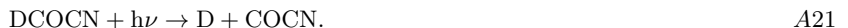
where,  $n_s$  is the surface density of sites,  $m$  is the mass of the adsorbed particle and  $E_d$  is the adsorption energy of the species. Here we use  $N_S=10^6$  and  $n_s = 2 \times 10^{14}$ .

Ice phase abundance of the surface species could be decreased by (a) thermal evaporation, (b) cosmic ray induced photo-dissociation and (c) cosmic ray induced evaporation process. Rate of thermal evaporation of the surface species 'i' could be calculated by the following relation;

$$k_{evap}(i) = \nu_0 \exp(-E_d/kT_g) \text{ sec}^{-1}, \quad (7)$$

where,  $E_d$  is the adsorption energy of the  $i^{th}$  species.

Following the Photo-dissociation channels of gas phase HCOCN, we have assumed that ice phase HCOCN & DCOCN could also be dissociated into the similar ways. So following, reaction A14 & A15, photo-dissociation channel of the ice phase DCOCN molecule could be as follows:



Moreover, we have assumed that Photo-dissociation rate of the surface species are same as in the gas phase (Eqn. 3).

Rate of cosmic ray induced evaporation are calculated by using the expression developed by Hasegawa & Herbst (1993). Hasegawa & Herbst (1993) did their simulation for gas and grain temperature 10K and for hydrogen number density =  $2 \times 10^4 \text{ cm}^{-3}$  cloud. Following Leger et al., (1985), they assumed that relativistic Fe nuclei with energies 20-70MeV could deposit 0.4 MeV energy on an average dust particle of radius  $0.1 \mu m$ . Now grain could be cooled down due to the thermal evaporation and radiation process. For the easy inclusion of cosmic ray induced photo-evaporation into their model, they developed the following relation:

$$k_{crd} \sim f(70, K) k_{evap}(i, 70K), \quad (8)$$

where,  $k_{evap}(i, 70K)$  is the thermal evaporation rate of the surface species 'i' at temperature 70K,  $f(70 K)$  is the fraction of the time spent by grains in the vicinity of 70K. Following Leger et al., (1985), they defined  $f(70K) = 3.16 \times 10^{-19}$ .

In our surface network, we have considered that the following reactions along with reaction number A1 for the production of HCOCN and DCOCN in the grain phase;



Reaction rate coefficients for the surface reactions (A1, A22, A23 & A24) are calculated by using Eqn. 3. Required adsorption energies for this calculations are mainly taken from Allen & Robinson (1977) and Hasegawa & Herbst (1993). Following Hasegawa, Herbst & Leung (1992), here also, we have assumed that  $E_b=0.3E_d$  except the case of atomic hydrogen. As like Hasegawa, Herbst & Leung (1992), here also we use,  $E_b=100\text{K}$  for atomic hydrogen. Binding energy of the deuterated species are assumed to be same as its hydrogenated counter part.

### 2.3 Spectral parameters

Quantum chemical calculations could be very accurate for the identification of several species in the interstellar medium. Huang & Lee (2008) proved that quantum chemical calculations might provide rotational constants often up to an accuracy of 20 MHz (especially for the B and C type constants) and also vibrational frequencies accurate to  $5 \text{ cm}^{-1}$  or better (Huang & Lee 2008, 2009, 2011; Huang et al. 2011; Inostroza et al. 2011; Fortenberry et al. 2011a, 2011b, 2012a, 2012b, 2012c). Following this type of earlier works, we are motivated to present the spectroscopic constants as well as the fundamental vibrational frequencies to assist in confirming detections of HCOCN and DCOCN in and around an ISM.

In order to study the spectroscopy of cyanoformaldehyde, we first optimize the geometry of the cyanoformaldehyde molecule at density functional theory based B3LYP method using 6-311++G\*\* basis set. Vibrational frequencies of cyanoformaldehyde and one of its isotopomer is computed by determining the second derivative of the energy with respect to the Cartesian nuclear coordinates and then transforming into mass-weighted coordinates. This transformation is valid only at a stationary point. Here, we are mainly considering the gas phase and the ice phase cyanoformaldehyde and one of its isotopomers. Properties of molecules and transition states can differ considerably between the gas phase and the solution phase. For example,

**Table 2.** Energies of the reactants, products and activated complex for the reaction  $\text{H}_2\text{CO} + \text{CN} \rightarrow \text{HCOCN} + \text{H}$  in the gas and ice phase.

Species	Gas phase SCF energy (Hartree)	Gas phase ZPE (Hartree)	Ice phase SCF energy (Hartree)	Ice phase ZPE (Hartree)
<b>H<sub>2</sub>CO</b>	-114.500430	0.026623	-114.507313	0.026722
<b>CN</b>	-92.707565	0.004675	-92.709497	0.004680
<b>TS</b>	-207.242371	0.035337	-207.239089	0.031268
<b>HCOCN</b>	-206.728293	0.026326	-206.737219	0.026364
<b>H</b>	-0.502257	0.000000	-0.502283	0.000000

the electrostatic effects are often much less important for species placed in a solvent with high dielectric constant than when they are in the gas phase (Foresman & Frisch, 1996). In our study, we consider simple as well as mixed ice. Simple ice consists of only water but the observational evidences suggest that  $\sim 90\%$  interstellar grain mantle is covered with  $\text{H}_2\text{O}$ ,  $\text{CH}_3\text{OH}$  and  $\text{CO}_2$  (Keane et al., 2001). This is why we also find the vibrational frequencies of these species by considering the actual percentage of the mixed solvent. The influence of the solvent in the vibrational spectroscopy of these species is done using the Polarizable Continuum Model (PCM) with the integral equation formalism variant (IEFPCM) as a default Self-consistent Reaction Field (SCRf) method. Among the different models, we have chosen IEFPCM model as a convenient one, since the second energy derivative is available for this model and also its analytic form is available. We also find the electronic absorption spectrum of HCOCN (for gas phase, ice phase and mixed ice phase) using the time dependent density functional theory (TDDFT study by IEFPCM model).

Rotational motion is commonly described by starting with the rigid rotor model. Calculations at the rotational level requires very higher level of basis sets for the better estimation of the structure and optimization. Here we use MP2/aug-cc-pVTZ level for performing our calculations. Some DFT methods with larger basis set could also be used as well. Corrections for the interaction between rotational motion and vibrational motion along with the corrections for vibrational averaging and an-harmonic corrections to the vibrational motion are also considered in our calculations. In brief, we report rotational constants for HCOCN, which are corrected for each vibrational state as well as vibrationally averaged structures. These rotational constants are needed to predict the spectrum of cyanoformaldehyde molecule and this can be done using the ‘SPCAT’ program (Pickett 1991). The SPCAT program requires two main files namely, ‘file.var’ and ‘file.int’. The ‘.var’ file is generated from quantum chemical simulations by using Gaussian 09W software. This file contains information about rotational constants, quadrupole coupling constants and distortion constants. The ‘.int’ file is the intensity file and it is prepared according to the prescribed format of ‘SPCAT program’. This file contains the maximum and minimum rotational states, partition function, rotational temperature and the dipole moment of the molecule.

## 2.4 Chemical Modeling

Our chemical model consists of a gas phase chemical network as well as the surface chemical network. Our gas phase chemical network consists of 5229 reactions among 591 species. This large gas phase network includes the network of Woodall (2007). In addition, we have introduced the formation and destruction pathways of cyanoformaldehyde, some important deuterated reactions following Robert & Millar, (2000) & Albertsson et al., (2011), and some reactions which lead to the formation of bio-molecules by following Chakrabarti & Chakrabarti (2000ab) & Majumdar et al. (2012). We assume that the gas and the grains are coupled through the accretion and thermal evaporation processes.

For the production of HCOCN on the grain surface, reactions A1 & A23 are considered. Along with these surface reactions, a large surface chemical network are used. Our surface chemical network consists of 285 surface reactions among 154 surface species. For this surface chemical network, we mainly have followed Hasegawa, Herbst & Leung (1992); Das et al., (2008); Das, Acharyya & Chakrabarti (2010); Das & Chakrabarti., (2011); Cazaux et al., (2010); Cuppen & Herbst (2007) & Stantcheeva et al., (2002). Binding energies of all the surface species are mainly taken from Allen & Robinson (1977) and Hasegawa & Herbst (1993). Binding energies of the deuterated species are assumed to be the same as its hydrogenated counter part. Here, we use parameters which are suitable to mimic a cold and dense interstellar cloud, namely  $T = 10 - 20\text{K}$ ,  $n_H = 2 \times 10^4 \text{ cm}^{-3}$ ,  $A_V = 10$  magnitude. Following Lee et al., (1996), in Table 1, initial fractional abundances relative to the total hydrogen nuclei is shown. This type of initial abundances are often adopted for the cold & dark cloud. Initial abundance of ‘D’ in the gas phase is varied from a concentration  $n_D = 0.001 \text{ cm}^{-3}$  to  $10 \text{ cm}^{-3}$ . This implies an initial deuterium fractionation of (atomic D/H ratio, hereafter  $R_D$ ) 0.001 – 10. Unless otherwise stated, following Caselli et al., (2002), we use  $R_D = 0.3$ .

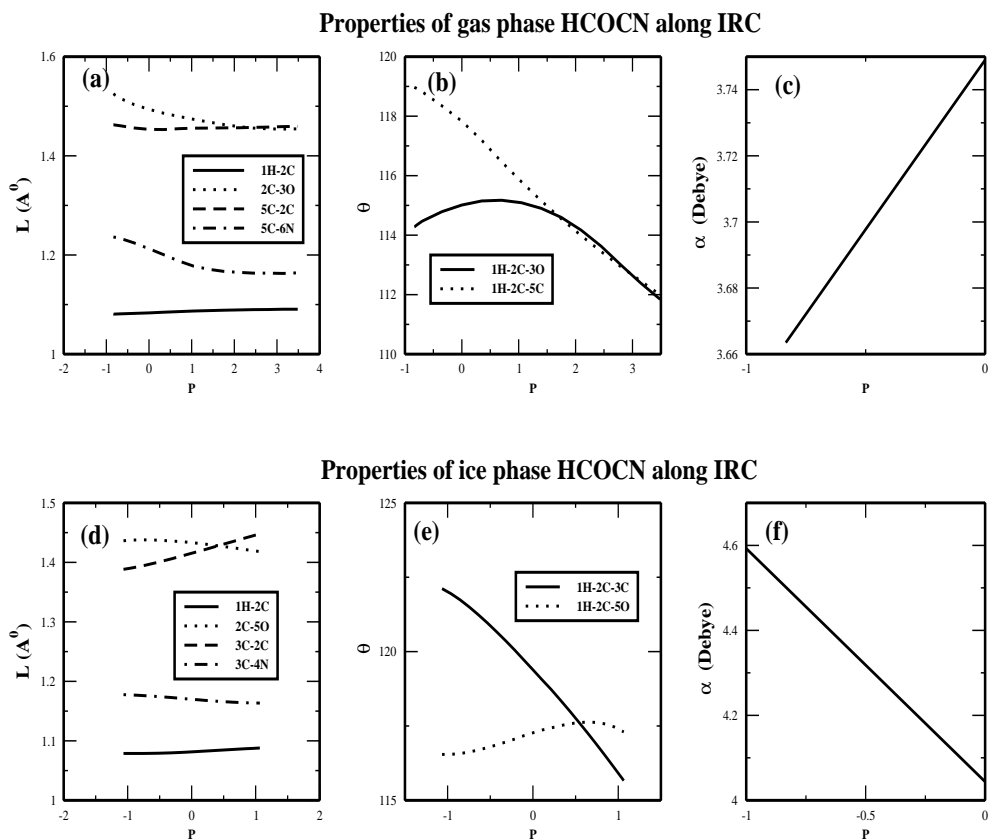


**Figure 1.** Variation of different Molecular properties for the formation of HCOCN in gas phase (a-c) and ice phase (d-f) with respect to the intrinsic reaction coordinate.

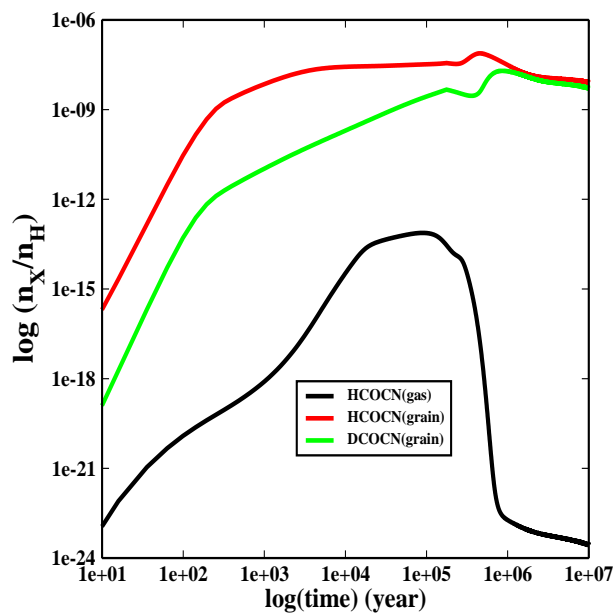


**Figure 2.** Time evolution of HCOCN and one of its isotopomer DCOCN in gas as well as in grains.

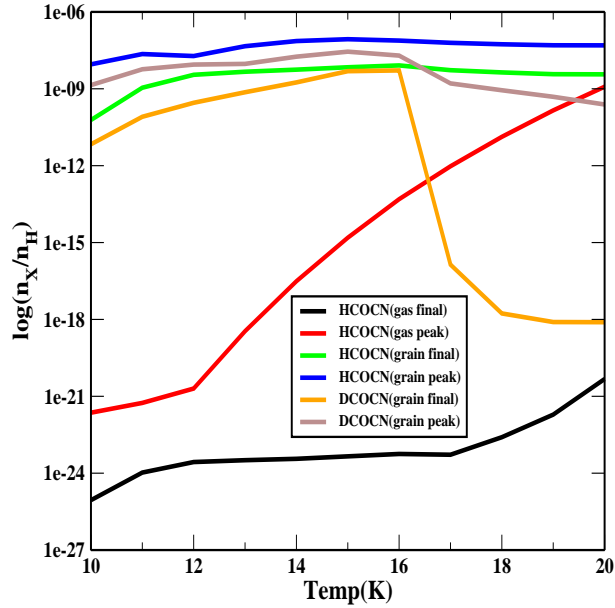


Figure 3. Variation of abundances with temperature.

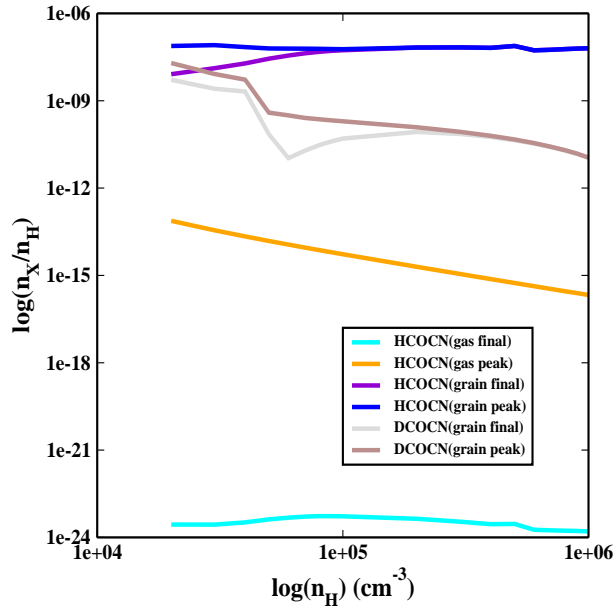


Figure 4. Variation of abundances with Hydrogen number density at 16K.

### 3 RESULTS AND DISCUSSIONS

#### 3.1 Chemical properties

In order to compute the energy of the transition structure of the reaction A1, we mainly perform three sets of calculations. First, we obtain the self-consistent field (SCF) energy by optimizing the transition structure geometry. Second, to obtain the zero point energy, we perform the frequency calculations and finally, we perform an Intrinsic Reaction coordinate (IRC) calculation. An IRC calculation examines the reaction path leading down from a transition structure on a potential energy surface and this is used as a composite variable, which spans all the degrees of freedom of the potential energy surface. Such



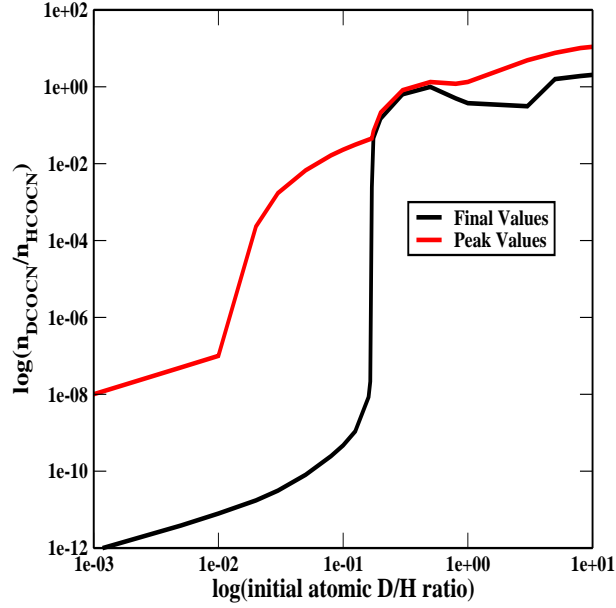


Figure 5. Deuterium fractionation of HCOCN, as a function of the initial D/H ratio.

Table 3. Rate coefficients

Reaction	Temperature (in K)	Gas phase reaction rates & type	Surface reaction rates
$\text{H}_2\text{CO} + \text{CN} \rightarrow \text{HCOCN} + \text{H}(\text{A1})$	16	$4.11 \times 10^{-11} \text{ sec}^{-1}$ (Radical-neutral)	$6.16 \times 10^{-7} \text{ sec}^{-1}$
$\text{H}_3^+ + \text{HCOCN} \rightarrow \text{H}_2\text{COCN}^+ + \text{H}_2(\text{A2})$	-	$2.85 \times 10^{-9} \text{ cm}^3\text{sec}^{-1}$ (Ion-molecular)	
$\text{C}^+ + \text{HCOCN} \rightarrow \text{HCO}^+ + \text{C}_2\text{N}(\text{A3})$	-	$1.53 \times 10^{-9} \text{ cm}^3\text{sec}^{-1}$ (Ion-molecular)	
$\text{C}^+ + \text{HCOCN} \rightarrow \text{CO} + \text{C}_2\text{NH}^+(\text{A4})$	-	$1.53 \times 10^{-9} \text{ cm}^3\text{sec}^{-1}$ (Ion-molecular)	
$\text{H}_3\text{O}^+ + \text{HCOCN} \rightarrow \text{H}_2\text{COCN}^+ + \text{H}_2\text{O}(\text{A5})$	-	$1.28 \times 10^{-9} \text{ cm}^3\text{sec}^{-1}$ (Ion-molecular)	
$\text{HCO}^+ + \text{HCOCN} \rightarrow \text{H}_2\text{COCN}^+ + \text{CO}(\text{A6})$	-	$1.1 \times 10^{-9} \text{ cm}^3\text{sec}^{-1}$ (Ion-molecular)	
$\text{HN}_2^+ + \text{HCOCN} \rightarrow \text{H}_2\text{COCN}^+ + \text{N}_2(\text{A7})$	-	$1.1 \times 10^{-9} \text{ cm}^3\text{sec}^{-1}$ (Ion-molecular)	
$\text{O}^+ + \text{HCOCN} \rightarrow \text{HCO}^+ + \text{OCN}(\text{A8})$	-	$1.36 \times 10^{-9} \text{ cm}^3\text{sec}^{-1}$ (Ion-molecular)	
$\text{H}^+ + \text{HCOCN} \rightarrow \text{CO}^+ + \text{HCN} + \text{H}(\text{A9})$	-	$4.85 \times 10^{-9} \text{ cm}^3\text{sec}^{-1}$ (Ion-molecular)	
$\text{H}^+ + \text{HCOCN} \rightarrow \text{HCO}^+ + \text{HCN}(\text{A10})$	-	$4.85 \times 10^{-9} \text{ cm}^3\text{sec}^{-1}$ (Ion-molecular)	
$\text{H}_2\text{COCN}^+ + \text{e}^- \rightarrow \text{CO} + \text{H}_2 + \text{CN}(\text{A11})$	-	$2 \times 10^{-7} \text{ cm}^3\text{sec}^{-1}$ (Dissociative Recombination)	
$\text{H}_2\text{COCN}^+ + \text{e}^- \rightarrow \text{HCO} + \text{H} + \text{CN}(\text{A12})$	-	$2 \times 10^{-7} \text{ cm}^3\text{sec}^{-1}$ (Dissociative Recombination)	
$\text{H}_2\text{COCN}^+ + \text{e}^- \rightarrow \text{HCOCN} + \text{H}(\text{A13})$	-	$2 \times 10^{-7} \text{ cm}^3\text{sec}^{-1}$ (Dissociative Recombination)	
$\text{HCOCN} + h\nu \rightarrow \text{HCO} + \text{CN}(\text{A14})$	-	$3.25 \times 10^{-17} \text{ sec}^{-1}$ (Photo-dissociation)	$3.25 \times 10^{-17} \text{ sec}^{-1}$
$\text{HCOCN} + h\nu \rightarrow \text{H} + \text{COCN}(\text{A15})$	-	$3.25 \times 10^{-17} \text{ sec}^{-1}$ (Photo-dissociation)	$3.25 \times 10^{-17} \text{ sec}^{-1}$
$\text{DCO} + \text{CN} \rightarrow \text{HCOCN} + \text{D}(\text{A22})$	16	-	$6.16 \times 10^{-7} \text{ sec}^{-1}$
$\text{HDCO} + \text{CN} \rightarrow \text{HCOCN} + \text{D}(\text{A23})$	16	-	$6.16 \times 10^{-7} \text{ sec}^{-1}$
$\text{D}_2\text{CO} + \text{CN} \rightarrow \text{DCO} + \text{D}(\text{A24})$	16	-	$6.16 \times 10^{-7} \text{ sec}^{-1}$

a calculation starts at the saddle point and follow the path in both the directions from the transition state by optimizing the geometry of the molecular system at each point along the path. Thus an IRC calculation connects two minima on the potential energy surface by a path which passes through the transition state between them. The energy of the reactants, products and activated complex with their corresponding zero point corrected values (in the unit of Hartree, 1 Hartree=27.211eV) are given in Table 2.

Fig. 1(a-f) shows the variation of different molecular parameters during the formation of HCOCN with respect to the intrinsic reaction co-ordinate (P) for the gas phase ( $\text{H}_2\text{CO}+\text{CN}\rightarrow\text{H}(1)\text{C}(2)\text{O}(3)\text{C}(5)\equiv\text{N}(6)+\text{H}$ ) as well as for the ice phase ( $\text{H}_2\text{CO}+\text{CN}\rightarrow\text{H}(1)\text{C}(2)\text{O}(5)\text{C}(3)\equiv\text{N}(4)+\text{H}$ ) by the reaction A1. Variation of the molecular parameters are shown in order to have the idea of the effect of solvent during any chemical reaction. Numbers in the parenthesis indicate the positions of the atoms during the reaction A1 in the gas phase as well as in the ice phase. Reaction paths of any chemical reactions are connected by the reactants and the products through its transition state. Fig. 1(a-c) shows the variation of bond length (L in  $\text{\AA}$ ), bond angle ( $\theta$  in degree) & dipole moment ( $\mu$  in Debye) along the IRC of the gas phase formation of HCOCN. Fig. 1(d-f) represent similar variations along IRC for the formation of HCOCN in the ice phase. In Fig. 1a, we show how the bond lengths (1H-2C, 2C-3O, 5C-2C & 5C-3O) vary. It is clear from the Figure that 5C-3O bond shows strong variation along the IRC. In case of Fig. 1d (ice phase HCOCN), we show similar variations for the 1H-2C, 2C-5O, 3C-2C & 3C-5O bond lengths. Bond lengths in the ice phase do not show any strong variation along IRC. In Fig. 1b, variations of bond angles (1H-2C-3O & 1H-2C-5C) are shown for the gas phase and in Fig. 1e, variations of bond angles (1H-2C-3C & 1H-2C-5O) are shown for the ice phase. In Fig. 1c and Fig. 1f, variations of Dipole moments are shown for the gas and ice phase respectively. Dipole moment for the gas phase shows a strong increasing slope for the formation of HCOCN, whereas for the ice phase formation of HCOCN, it shows a strong decreasing slope along IRC. Increasing slope of the dipole moment in the gas phase could be explained due to a substitution of the H atom by a more electronegative group (-CN) whereas a decreasing slope of the ice phase could be explained due to the increase of the of 3C-2C bond and the increase of  $\angle 1\text{H}-2\text{C}=5\text{O}$  bond angle (Fig.1d and Fig.1e respectively) and due to the strong interaction with the solvent.

Calculation of gas phase rate coefficients are already discussed in Section 2.1. Rate coefficients for the gas phase reaction A1 are calculated by using free energy of activation (using Eqs. 1) and the rate coefficients for the ion-molecular reactions(A2-A10) are calculated using the capture theories(Eqn. 2). In Table 3, we have summarized all the calculated/assumed rate coefficients for the formation/destruction of HCOCN and DCOCN in gas/ice phase.

### 3.2 Chemical evolution & deuterium enrichment

Rate coefficients for the surface reactions are calculated by following the procedure discussed in the Section 2.2. According the discussion above, binding energies are the key for the surface reactions. For the production of HCOCN, it is essential to have a knowledge about the binding energies of the reactants with the grain surface. Following Allen & Robinson (1977), we use adsorption energies of  $\text{H}_2\text{CO}$  and  $\text{CN}$  3.5 Kcal mole<sup>-1</sup> and 3 Kcal mole<sup>-1</sup> respectively. Adsorption energies of HDCO and  $\text{D}_2\text{CO}$  are assumed to be similar to the  $\text{H}_2\text{CO}$  molecule. In Table 3, the calculated rate coefficients are tabulated in sec<sup>-1</sup> for 16K cloud. Now in order to have an idea about the abundances of the HCOCN and DCOCN around the dense interstellar cloud, we ran several cases and all the relevant abundances are presented with respect to the total hydrogen. In Fig. 2, the time evolution of HCOCN abundance in the gas phase & ice phase along with the DCOCN abundance in the ice phase are shown for T=16K,  $A_V=10$ ,  $n_H = 2 \times 10^4 \text{ cm}^{-3}$  and  $R_D = 0.3$ .

In the gas phase, production of HCOCN molecule is significant but HDCO or  $\text{D}_2\text{CO}$ , which are required to form DCOCN (Eqn. A22 & A24) are not abundant in the gas phase. Due to this reason, we do not consider the production of DCOCN in our gas phase chemical network. In the ice phase, HDCO or  $\text{D}_2\text{CO}$  could be produced efficiently, which then react with CN radical to form DCOCN (reaction A22 and A24). From Fig. 2, it is clear that HCOCN could be efficiently produced in the gas phase having peak abundance  $7.51 \times 10^{-14}$ . It is distinctly clear from Fig. 2, that HCOCN and DCOCN both are significantly abundant on the grain surface having peak abundance  $7.61 \times 10^{-8}$  and  $1.98 \times 10^{-8}$  respectively.

Here, we mainly concentrate on the temperature range of 10 – 20K to mimic the dense cloud condition. Due to the exponential dependency of the gas phase rate coefficient (Eqn. 1) on temperature, the rate coefficient sharply rises with temperature of the gas. This, in turn, increases the production of gas phase HCOCN. In Fig. 3, the peak abundances of the gas phase HCOCN, ice phase HCOCN and DCOCN as well as the final abundances (by final abundance, we want to mean the abundance after the life time  $\sim 10^7$  years of a molecular cloud) of these species with respect to the temperature are shown. For this case, we consider  $n_H = 2 \times 10^4 \text{ cm}^{-3}$ ,  $A_V = 10$  and vary the temperature from 10K to 20K. Abundance of the gas phase HCOCN (peak values as well as the final values) increases sharply due to the enhancement of the rate coefficient with temperature. Its peak abundance varies from  $2.3 \times 10^{-22}$  to  $1.21 \times 10^{-9}$  as the temperature is increased from 10K to 20K, whereas the final abundance of gas phase HCOCN varies from  $8.84 \times 10^{-26} \text{ cm}^{-3}$  to  $4.72 \times 10^{-21}$  in between the specified temperature range. Surface production of HCOCN or DCOCN depends upon the surface population of  $\text{H}_2\text{CO}$ , HDCO,  $\text{D}_2\text{CO}$  and CN molecules. As the temperature increases, the thermal hopping time scale (Eqn. 5) would be much shorter, which makes the sweeping rate to be much faster. But as the thermal evaporation time scale also decreases with the temperature,

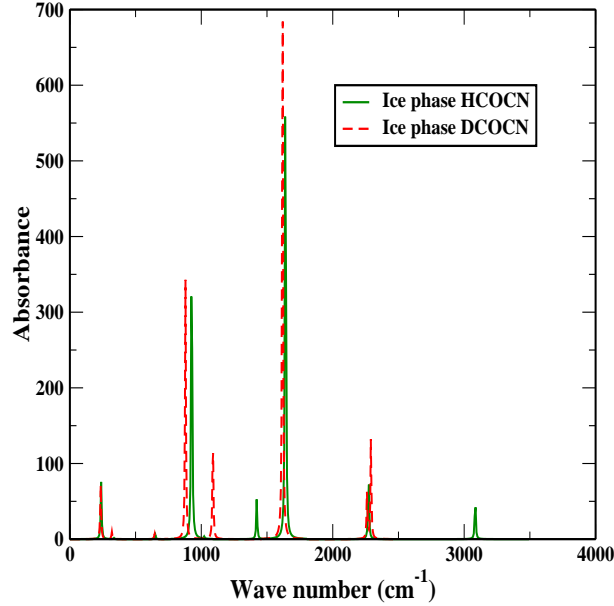


Figure 6. Infrared spectrum of HCOCN and DCOCN in water ice.

residential time of the H or D atoms on the grain surface decreases. Moreover, there are always a competition going on between the H and the D atoms. As we have considered  $R_D = 0.3$  for this case, abundance of H atom is a bit higher compare to the D atom, that is why final abundance of HCOCN does not show a drastic drop as in the case of the final surface abundance of DCOCN (Fig. 3). The peak values of the ice phase HCOCN abundance oscillates between  $8.97 \times 10^{-9} - 4.94 \times 10^{-8}$  and the peak values of the ice phase DCOCN abundance oscillates between  $1.40 \times 10^{-9} - 2.44 \times 10^{-10}$ . Whereas, the final values of ice phase HCOCN oscillates between  $6.07 \times 10^{-11} - 3.67 \times 10^{-9}$  and the final values of ice phase DCOCN oscillates between  $6.83 \times 10^{-12} - 7.80 \times 10^{-19}$ .

Remijan et al., (2008) made a few simple assumptions while computing the HCOCN abundances. According to them, the gas phase HCOCN abundance could be  $4 \times 10^{-9}$  with respect to the total hydrogen. Following the work of Lewis-Bevin et al., (1992) they considered that Cyanoformaldehyde could be destroyed by reacting with  $H_2O$  molecules. Assuming that the formation of Cyanoformaldehyde is dominated mainly by the reaction of CN with  $H_2CO$  with a rate of  $k_1$ , and that its destruction is due to the reaction with  $H_2O$  with a rate  $k_2$ , they determined the relative cyanoformaldehyde abundance ratio as  $X(\text{Cyanoformaldehyde}) \sim k_1 X(\text{CN})X(\text{H}_2\text{CO})/k_2 X(\text{H}_2\text{O})$ ; with  $X(\text{CN}) \sim X(\text{H}_2\text{CO}) \sim 2 \times 10^{-8}$ ,  $X(\text{H}_2\text{O}) \sim 1 \times 10^{-7}$ , and  $k_1 \sim k_2$ ,  $X(\text{CNCHO}) 4 \times 10^{-9}$ . In our case, we mentioned that the heat of formation for the reaction between Cyanoformaldehyde and water (reaction A5) is 60 KJ/mole, so this reaction is not feasible around the dense cloud region. Moreover Remijan et al., (2008) considered that the formation rate of Cyanoformaldehyde( $k_1$ ) is equal to the destruction rate ( $k_2$ ). This assumption could be very inaccurate. Remijan et al.,(2008) also derived the column density of HCOCN from the data derived by Martin et al., (2004). According to their calculations, HCOCN abundance would be in the range  $(0.7 - 11) \times 10^{-9}$  for a molecular hydrogen column density of  $1.6 \times 10^{23} \text{ cm}^{-2}$  and column density would be in the range of  $(1 - 17) \times 10^{14} \text{ cm}^{-2}$ .

Following Shalabiea et al., (1994) and Das & Chakrabarti (2011), the column density of a species could be calculated by the following relation;

$$N(A) = n_H x_i R, \quad (9)$$

where,  $n_H$  is the total hydrogen number density,  $x_i$  is the abundance of the  $i^{\text{th}}$  species and  $R$  is the path length along the line of sight ( $= \frac{1.6 \times 10^{21} \times A_V}{n_H}$ ).

In Fig. 4, we show the abundance variation of the gas phase HCOCN, ice phase HCOCN and ice phase DCOCN at  $T = 16\text{K}$  with respect to the variation of the number density of the cloud in between  $n_H = 2 \times 10^4 \text{ cm}^{-3} - 10^6 \text{ cm}^{-3}$ . Gas phase abundance of HCOCN shows a decreasing trend with the increase in the number density of the cloud. Peak value of the gas phase HCOCN decreases from  $7.51 \times 10^{-14}$  to  $2.12 \times 10^{-16}$  for the change of number density from  $2 \times 10^4 \text{ cm}^{-3}$  to  $10^6 \text{ cm}^{-3}$ . From Eqn. 9, these abundances result in the peak column density of  $1.20 \times 10^9 \text{ cm}^{-2}$  to  $3.39 \times 10^6 \text{ cm}^{-2}$ , which is beyond the observational limit. The behaviour of the grain phase production is more interesting. Final value of ice phase HCOCN shows an increasing trend up to  $n_H \sim 10^5 \text{ cm}^{-3}$ . Beyond that, the abundances remain roughly constant even when the number

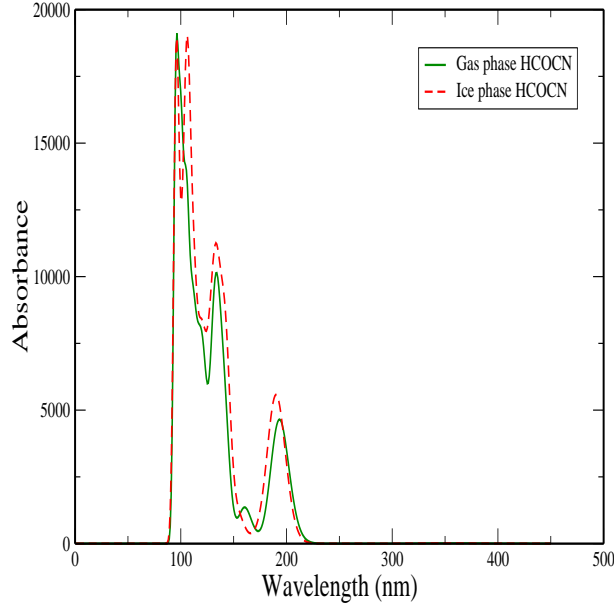


**Figure 7.** Electronic absorption spectrum of HCOCN in gas well as in ice phase.

density of the cloud is raised by an order of magnitude. Beyond  $10^5 \text{ cm}^{-3}$ , final abundance of ice phase HCOCN and peak value roughly overlaps. In between, the density range considered here, the peak value of the ice phase HCOCN fluctuates between  $7.61 \times 10^{-8}$  to  $6.38 \times 10^{-8}$ , which corresponds to the column density of  $1.22 \times 10^{15} \text{ cm}^{-2}$  to  $1.02 \times 10^{15} \text{ cm}^{-2}$ . In case of ice phase DCOCN, peak value decreases with the increase in the number density of the cloud, whereas initially decreasing trend was observed for for the final values of DCOCN. Beyond  $2 \times 10^5$  year, final values and peak values follow the same decreasing trend. Peak value of the ice phase DCOCN for  $2 \times 10^4 \text{ cm}^{-3}$  cloud was  $1.98 \times 10^{-8}$  which reaches  $1.12 \times 10^{-11}$  for the  $10^6 \text{ cm}^{-3}$  number density cloud. This implies a column density of  $3.17 \times 10^{14} - 1.79 \times 10^{11} \text{ cm}^{-2}$ .

Around the low extinction region ( $A_V < 5$ ), the chemical composition is heavily affected by the interstellar photon (Das & Chakrabarti, 2011). Das & Chakrabarti (2011), also showed that if we assume that the number density of the cloud does not vary with the extinction for  $A_V > 10$  then the ice composition does not vary at all. Now if we considered, say,  $A_V \sim 145$  (a value considered by Allamandola et al., 1992 for W33A) for the case of Fig. 4, then the computed abundances would not show any significant variations. But while we would transform this abundances into column densities by Eqn. 8 there would be an increase in the column densities by a factor of 14.5. So, in between the density range  $2 \times 10^4$  to  $10^6 \text{ cm}^{-3}$ ,  $T=16\text{K}$  and for  $A_V=145$ , a peak column density of gas phase HCOCN comes out to be  $1.74 \times 10^{10} \text{ cm}^{-2}$ , whereas peak column densities of the ice phases of HCOCN and DCOCN come out to be  $1.77 \times 10^{16} \text{ cm}^{-2}$  and  $4.6 \times 10^{15} \text{ cm}^{-2}$  respectively. It is well known that if some energetic events occur, then most of the surface species would get lost from the surface and populate the gas phase. Since here we are considering that the temperature remains the same ( $T = 16\text{K}$ ) in the simulation time scale, most of the complex surface species once produced/accreted get trapped into the potential well of the grain surface. Only some percentage of the species could be evaporated by the thermal evaporation (Eqn. 5) or cosmic ray induced evaporation process (Eqn. 6). But these are not efficient enough to populate the gas phase. Our calculated ice phase column densities are in line with the gas phase abundance prediction of Remijan et al., (2008), who used the data derived by Martin et al., (2004).

To check the fractionation of HCOCN, we vary the initial gas phase atomic ratio of D/H ( $R_D$ ) of the cloud in the range from 0.001 to 10 by keeping all other initial parameters the same at  $n_H = 2 \times 10^4 \text{ cm}^{-3}$ ,  $T = 16\text{K}$ ,  $A_V=10$ . In Fig. 5, we plot the DCOCN and HCOCN abundance ratio(peak and final values) in the ice phase with respect to the initial gas phase D/H ratio. As expected, the ratio increases with the increase of the atomic deuterium abundance in the gas phase. For the high value of initial gas phase D/H ratio, the fractionation of HCOCN ( $> 1$ ) exceeds the cosmic D/H ratio of  $1.5 \times 10^{-5}$  (Roberts & Millar 2000). From Fig.5, it is evident that the peak value of the fractionation ratio greater than 1 for initial D/H ratio  $> 0.4$ . Looking at the abundances of the DCOCN, we would thus expect to observe DCOCN in the ISM as well.

**Table 4.** Vibrational frequencies of Cyanoformaldehyde molecule and one of its isotopomer in gas phase, H<sub>2</sub>O ice, methanol ice and mixed water ice at B3LYP/6-311G+\*\* level of theory

Species	Peak positions (Gas phase) (in cm <sup>-1</sup> )	Absorbance	Peak positions (H <sub>2</sub> O ice) (in cm <sup>-1</sup> )	Absorbance	Peak positions (Mixed ice) (in cm <sup>-1</sup> )	Absorbance
HCOCN	237.18	12.69	238.11	21.92	238.32	21.00
	331.41	0.17	336.27	0.43	335.80	0.41
	648.66	1.88	649.40	1.90	649.59	1.90
	938.68	92.42	927.01	145.40	927.82	140.88
	1019.28	0.31	1022.82	0.84	1022.80	0.80
	1421.46	7.71	1421.99	16.15	1421.41	15.32
	1655.43	128.64	1640.47	223.04	1641.74	214.43
	2269.21	31.24	2272.50	28.10	2272.22	29.39
	3033.11	33.56	3084.17	18.21	3080.19	19.37
	DCO CN	233.40	12.33	234.34	21.31	234.52
315.40		1.53	319.79	2.78	319.39	2.66
643.59		1.94	644.26	2.01	644.44	2.09
876.02		0.59	876.81	0.53	877.00	0.54
888.25		61.95	879.59	99.89	880.07	96.48
1089.94		26.67	1087.86	42.18	1087.70	41.06
1635.75		131.39	1618.37	230.78	1619.90	221.60
2234.33		24.91	2260.81	18.19	2259.45	18.03
2274.29		42.69	2290.78	39.28	2288.78	40.41

### 3.3 Spectral Analysis

We now turn to the spectral properties. For this, we need to compute the infrared peak positions with their absorbance in the gas phase as well as in ice and mixed ice phase. In Table 4, we present these for HCOCN and one of its isotopomers, namely, DCOCN. We find that the most intense mode of HCOCN in the gas phase appears nearly at 1655.43 cm<sup>-1</sup>. This peak is shifted in the ice phase (water ice) by nearly 15 cm<sup>-1</sup> and appears at 1640.47 cm<sup>-1</sup>. The second strongest peak in the gas phase appears at 938.68 cm<sup>-1</sup>. It is also shifted in the ice phase. To have a more realistic condition, instead of only water ice, we consider a mixed ice mantle, which contains 70% water, 20% methanol and 10% CO<sub>2</sub> molecules (Keane et al., 2001; Das & Chakrabarti, 2011). For the pure water ice, Gaussian 09W uses a dielectric constant of  $\sim 78.5$  by default. For the mixed ice, we put the dielectric constant of the medium to be 61, which is calculated by taking the weighted average of the dielectric constants of H<sub>2</sub>O, CH<sub>3</sub>OH and CO<sub>2</sub>. We note that the most intense peak in the gas phase is shifted in the mixed ice also (Table 4). Isotope effects on the chemical shifts is caused by differences in vibrational modes due to the different isotope masses. Each of the HCOCN and DCOCN has a unique spectrum because the substitution of the isotope changes the reduced mass of the corresponding molecule. We find that the most intense mode of DCOCN in the gas phase appears at 1635.75 cm<sup>-1</sup>. This peak is shifted in the ice phase by 17.35 cm<sup>-1</sup>, i.e., at 1618.37 cm<sup>-1</sup>. The second strongest peak in the gas phase which appears at 888.25 cm<sup>-1</sup> is also shifted in the ice phase and appears at 879.59 cm<sup>-1</sup>. The most intense peak in the gas phase is similarly shifted in the mixed solvated grain. Infrared peak positions with their absorbance in the gas phase as well as in the ice and mixed ice phase are pointed for the DCOCN in Table 4. In Fig. 6, we show how the isotopic substitution (DCO CN) plays a part in the vibrational progressions of HCOCN in the ice phase. In Table 5, we summarize the experimental values of the rotational and quartic centrifugal distortion constants from Bogey et al. (1988) and our calculated rotational and distortional constants of HCOCN molecule. Calculated constants are corrected for each vibrational state as well as the vibrationally averaged structures. Here we use MP2/aug-cc-pVTZ level to perform this calculations for the gas phase HCOCN molecule. In Table 5, calculated distortional constants along with the Experimental Quartic Centrifugal distortion constants correspond to I<sup>1</sup> representation with ‘A’ reduction are tabulated. Calculated rotational constants (B and C) are in very good agreement with the measured values. Our calculated values of B and C varies by 35 MHz and 29 MHz respectively from the experimentally obtained B and C values. Other distortional constants ( $\Delta_J$ ,  $\Delta_{JK}$ ,  $\Delta_K$ ,  $\delta_j$ ,  $\delta_k$ ) are relatively closer to the experimentally obtained values. Measured value of A deviates significantly from our calculated value. This difference could be explained due to the difference between the techniques involved. Calculation of rotational constants refer to an equilibrium geometry, while the measured ones are subject to some vibrational effects also (Csaszar, 1989). Calculated distortional constants in the asymmetrically reduced Hamiltonian are very close to the measured quartic centrifugal rotational constants. In order to summarize the outcome of our calculations about the rotational spectroscopy, we have prepared our spectral information as per the guidelines of the JPL (Table 7 of Appendix A).

Different electronic absorption spectral parameters of HCOCN in the gas phase are given in Table 6. In the gas phase, the spectrum is characterized by four intense peaks at the wavelengths 193.7, 160.5, 133.9, 96.7 nm (Fig. 7). These intense peaks are assigned due to the Highest occupied molecular orbital (HOMO)- Lowest unoccupied molecular orbital (LUMO) transitions. These transitions correspond to H-1 $\rightarrow$  L+0, H-0 $\rightarrow$  L+2, H-2 $\rightarrow$  L+1 and H-3 $\rightarrow$  L+9. Depending on the composition of the

**Table 5.** Theoretical & Experimental rotational parameters of Cyanoformaldehyde molecule

Species	Rotational constants	Values in MHz	Experimental values in MHz <sup>a</sup>	Distortional constants	Values in MHz	Experimental values in MHz <sup>a</sup>
HCOCN in gas phase	A	66034.4	67473.54	$\Delta_J$	$2.267 \times 10^{-3}$	$2.266 \times 10^{-3}$
	B	4975.9	5010.19	$\Delta_{JK}$	-0.1413	-0.143104
	C	4627.1	4656.498	$\Delta_K$	7.074	8.99
				$\delta_j$	$3.933 \times 10^{-4}$	$3.877 \times 10^{-4}$
				$\delta_k$	0.02895	0.034325

<sup>a</sup> Bogey et al., (1988)**Table 6.** Electronic transitions of cyanoformaldehyde molecule at B3LYP/6-311++G\*\* level

Species	Wavelength in nm	Absorbance	Oscillator strength	Transitions	Contribution in %
HCOCN	193.7	4651	0.1051	H-1 → L+0	85
	160.5	1360	0.032	H-0 → L+2	94
	133.9	10128	0.1234	H-2 → L+1	63
	96.7	19111	0.0458	H-3 → L+9	44
HCOCN in pure H <sub>2</sub> O ice	190.7	5561	0.1307	H-1 → L+0	85
	133.2	11260	0.1603	H-2 → L+1	60
	108.3	17562	0.0045	H-2 → L+6	96
	95.3	18507	0.2275	H-0 → L+13	34
HCOCN in mixed ice	191.2	5618	0.1348	H-1 → L+0	86
	135.4	11327	0.0528	H-0 → L+5	92
	108.5	17667	0.0048	H-2 → L+6	96
	98.1	16680	0.0289	H-4 → L+5	89

interstellar grain mantle peak positions in the ice phase are shifted. These features are given in the Table 6 with corresponding transition details. Fig. 7 clearly shows some differences in the gas phase and ice phase electronic absorption spectra.

#### 4 CONCLUSIONS

Recently, there were some indications of observations of HCOCN molecules inside molecular clouds. In this paper, we have investigated different aspects of the abundance of HCOCN in the ISM. They are:

- We perform a quantum chemical calculation to find out the realistic rate coefficient for the formation of HCOCN molecule around the cold, dense cloud.
- Our chemical modeling shows that HCOCN and DCOCN could efficiently be formed in the ice phase. We are proposing that this molecule may be observed in the ice phase as well.
- By introducing a large deuterated network into our chemical model, we have explored the possibility of studying one of the isotopologues (DCOHN) of HCOCN. We notice that DCOHN is produced very efficiently in the ice phase. By varying the model parameters, we find that the fractionation ratio of HCOCN could be greater than 1 (Fig. 5). Our Model calculation shows that maximum column density of ice phase HCOCN could be reached up to  $4.64 \times 10^{15} \text{ cm}^{-2}$  and for DCOHN it could be reached up to  $3.34 \times 10^{14} \text{ cm}^{-2}$  in the density range of  $2 \times 10^4 - 10^6 \text{ cm}^{-3}$ .
- We explore the vibrational and electronic spectral properties of HCOCN in different astrophysical conditions (such as, in the gas phase, ice phase and mixed ice phase). Different rotational & distortional constants for the gas phase HCOCN are tabulated and compared with the experimentally obtained values. Moreover, in the Appendix A, we prepare a catalog file in JPL format for the gas phase HCOCN molecule which will be helpful for the observer. Our result could be used as a guide to observers to look for this species in or around various molecular clouds.
- Based on certain observational results, we assumed grain mantles of different compositions. We considered grain mantles mainly composed of pure water. We also assumed the possibility that the ice mantle could be mixed in nature, consisting of water, methanol and carbon dioxide, for example. Based on the earlier studies, we assumed that the interstellar grain mantle consists of 70% water, 20% Methanol and 10% CO<sub>2</sub>. We tabulated the differences in spectral properties due to the different types of ices. Future observations are expected to explore the composition of the ice mantle based on which our result may be revised further.

## 5 ACKNOWLEDGMENTS

We would like to thank the anonymous referees whose valuable suggestions have helped to improve this paper a lot. Ankan Das is grateful to ISRO for the financial support through a respond project (Grant No. ISRO/RES/2/372/11-12) and SC, SKC, RS, and LM thank a DST project (Grant No.SR/S2/HEP-40/2008).

## REFERENCES

- Aikawa, Y., Herbst, E., Roberts, H., Caselli, P., 2005. *ApJ* 620, 330.
- Allamandola L. J., Sandford S. A., Tielens, A. G. G. M., 1999, *ApJ*, 399, 134
- Allamandola L. J., Hudgins D. M., Sandford S. A., 1999, *ApJ*, 511, L115
- Albertsson, T., Semenov, D. A., Henning, T., 2011, ASSA, eprint arXiv:1110.2644
- Allen, M., Robinson, G. W., 1977., *ApJ*, 212, 396
- Balucani, N., Asvany, O., Kaiser, R. I., Osamura, Y., *J. Phys. Chem. A*, 106, 4301
- Becke A. D., 1993, *J. Chem. Phys.*, 98, 5648
- Bogey, M., Destombes, J. L., Vallee, Y., Ripoll, J. L., *Chem. Phys. Letters* 146, 227
- Caselli, P., Stantcheva, T., Shalabiea, O., Shematovich, V. I. & Herbst, E., 2002, *P&SS*, 50, 1257
- Csaszar, A., G., *Chemical Physics Letter*, 1989, 162, 4
- Cazaux, S., Cobut, V., Marseille, M., Spaans, M., Caselli, P. 2010, *A&A*, 522, 74
- Chakrabarti, S., Chakrabarti, S.K., 2000a. *A&A* 354, L6
- Chakrabarti, S. K., Chakrabarti, S., 2000b. *Ind. J. Phys* 74B, 97
- Chakrabarti, S.K., Das, A., Acharyya, K., Chakrabarti, S., 2006, *A&A*, 457, 167
- Chakrabarti, S.K., Das, A., Acharyya, K., Chakrabarti, S., 2006, *BASI*, 34, 299
- Churchwell, E. 1980, *ApJ*, 240, 811
- Clouthier, D. J., Moule, D.C., 1987, *J. Am. Chem. Soc.* 109, 6259
- Cuppen, H. M., Herbst, E., 2007, *APJ*, 668, 294
- Cuppen, H. M., Van Dishoeck E., F., Herbst, E., Tielens, A. G. G. M., 2009, *A&A*, 508, 275
- Das, A., Acharyya, K., Chakrabarti, S. & Chakrabarti, S. K., 2008b, *A&A*, 486, 209
- Das, A., Acharyya, K. & Chakrabarti, S. K., 2010, *MNRAS* 409, 789
- Das, A., Chakrabarti, S. K., Acharyya K. & Chakrabarti, S., 2008a, *NEWA*, 13, 457
- Das, A. & Chakrabarti, S. K., 2011, 418. 545, *MNRAS*
- Das, A. Majumdar, L., Chakrabarti, S. K., & Chakrabarti S., 2013, *NEWA*, 23, 118
- Foresman, J.B., Frisch, A., 1995-96, *Exploring Chemistry with Electronic structure methods*, Gaussian, Inc., Pittsburgh, PA, 15106 USA
- Fortenberry, R. C., Crawford, T. D. 2011a, *Annu. Rep. Comput. Chem.*, 7, 195
- Fortenberry, R. C., Crawford, T. D. 2011b, *JPCA*, 115, 8119
- Fortenberry, R. C., Huang, X., Francisco, J. S., Crawford, T. D., Lee, T. J., 2012a, *JPCA*, 116, 9582
- Fortenberry, R. C., Huang, X., Francisco, J. S., Crawford, T. D., Lee, T. J., 2012b, *JChPh*, 136, 234309
- Fortenberry, R. C., Huang, X., Francisco, J. S., Crawford, T. D., Lee, T. J., 2012c, *JChPh*, 136, 234309
- Gerin, M., Combes, F., Encrenaz, P., Turner, B., Wootten, A., Bogey, M., Destombes, J.L., 1989, *A&A*, 224, L24-L26
- Hasegawa, T., Herbst, E., Leung, C.M., 1992, *APJ*, 82, 167
- Hasegawa, T., Herbst, E., 1993, *MNRAS*, 261, 83
- Herbst, E., 1996, *Atomic, Molecular, & Optical Physics Handbook*, edited by G. W. F. Drake, AIP Press, New York, 429, 36
- Huang, X., Lee, T. J. 2008, *JChPh*, 129, 044312
- Huang, X., Lee, T. J. 2009, *JChPh*, 131, 104301
- Huang, X., Lee, T. J. 2011, *ApJ*, 736, 33
- Inostroza, N., Huang, X., Lee, T. J. 2011, *JChPh*, 135, 244310
- Jalbout, A. F., Shipar, M. A. H., 2008, *J. Chem. Sci.*, 120, 329
- Judge, R. H., Moule, D. C., Biernacki, A., Benkel, M., Ross, J. M. Rustenburg, J., 1986, *J. Mol. Spectrosc.*, 116, 364
- kaiser, R. I., Ochsenfeld, C., Head-Gordon, M., Lee, Y. T., 1999, *APJ*, 510, 784
- Keane, J. V., Boogert, A. C. A., Tielens, A. G. G. M., Ehrenfreund, P., Schutte, W. A., 2001, *A&A*, 375L, 43
- Lee, H. H., Herbst, E., Forets, G. P., Roueff, E., Bourlot, J. L., 1996, *A&A*, 311, 690
- Leger, A., Jura, M, Omont, A., 1985, *A&A*, 144, 147
- Lewis-Bevan, W., Gaston, R.D., Tyrrell, J., Stork, W.D., Salmon, G.L., 1992, *J. Am. Chem. Soc.*, 114, 1933
- Majumdar, L., Das, A., Chakrabarti, S.K., Chakrabarti, S., 2013, *New Astronomy*, 20, 15
- Majumdar, L., Das, A., Chakrabarti, S.K., Chakrabarti, S., 2012, *Research in Astronomy & Astrophysics*, 12, 1613
- Martin, C. L., Walsh, W. M., Xiao, K., Lane, A. P., Walker, C. K., Stark, A. A., 2004, *APJS*, 150, 239

- Muller, H. S. P., Schloder, F., Stutzki, J., & Winnewisser, G. 2005, *J. Mol. Struct.*, 742, 215  
Muller, H. S. P., Thorwirth, S., Roth, D. A., & Winnewisser, G. 2001, *A&A*, 370, L49  
Pickett, H. M., *J. Mol. Spectrosc.*, 1991, 148, 371  
Remijan, A.J., Hollis, J.M., Lovas, F.J., Stork, W.D., Jewell, P.R., Meier, D.S., 2008, *APJ*, 675: L85  
Roberts, H., Millar, T. J., 2000, *A&A*, 361, 388  
Shalabiea, O. M., greenberg, J. M., 1994, *A&A*, 290, 266  
Stantcheva, T., Shematovich, V. I., Herbst, E., 2002, *A&A*, 391, 1069  
Woodall, J., Agnèz, M., Markwick-Kemper, A.J., Millar, T.J., 2007, *A&A*, 466, 1197  
Zuckerman, B., & Palmer, P. 1974, *ARA&A*, 12, 279



**Appendix-A**

**Table 7.** Different rotational transitions and its related parameters for gas phase cyanofomaldehyde molecule in the format of JPL catalog.

Frequency <sup>a</sup>	Uncertainty <sup>b</sup>	I <sup>c</sup>	D <sup>d</sup>	E <sub>lower</sub> <sup>e</sup>	g <sub>up</sub> <sup>f</sup>	Tag <sup>g</sup>	QnF <sup>h</sup>	Qn <sub>up</sub> <sup>i</sup>	Qn <sub>lower</sub> <sup>j</sup>
9602.0577	0.0000	-7.3358	3	-0.0000	3	55001	304	1 0 1 1	0 0 0 1
9603.2441	0.0000	-7.1139	3	-0.0000	5	55001	304	1 0 1 2	0 0 0 1
9605.0238	0.0000	-7.8128	3	-0.0000	1	55001	304	1 0 1 0	0 0 0 1
19204.8519	0.0000	-7.0358	3	0.3203	5	55001	304	2 0 2 2	1 0 1 2
19205.0496	0.0000	-6.9108	3	0.3204	3	55001	304	2 0 2 1	1 0 1 0
19206.0382	0.0000	-6.5586	3	0.3203	5	55001	304	2 0 2 2	1 0 1 1
19206.1230	0.0000	-6.2875	3	0.3203	7	55001	304	2 0 2 3	1 0 1 2
19206.8293	0.0000	-8.2117	3	0.3203	3	55001	304	2 0 2 1	1 0 1 2
19208.0157	0.0000	-7.0357	3	0.3203	3	55001	304	2 0 2 1	1 0 1 1
28807.6502	0.0000	-6.8613	3	0.9610	7	55001	304	3 0 3 3	2 0 2 3
28808.7236	0.0000	-6.1289	3	0.9610	5	55001	304	3 0 3 2	2 0 2 1
28808.9213	0.0000	-5.9582	3	0.9609	7	55001	304	3 0 3 3	2 0 2 2
28808.9684	0.0000	-5.7979	3	0.9610	9	55001	304	3 0 3 4	2 0 2 3
28809.4299	0.0000	-8.4052	3	0.9610	5	55001	304	3 0 3 2	2 0 2 3
28810.7010	0.0000	-6.8613	3	0.9609	5	55001	304	3 0 3 2	2 0 2 2
38410.3229	0.0000	-6.7387	3	1.9219	9	55001	304	4 0 4 4	3 0 3 4
38411.5564	0.0000	-5.6807	3	1.9220	7	55001	304	4 0 4 3	3 0 3 2
38411.6412	0.0000	-5.5626	3	1.9219	9	55001	304	4 0 4 4	3 0 3 3
38411.6711	0.0000	-5.4474	3	1.9219	11	55001	304	4 0 4 5	3 0 3 4
38412.0179	0.0000	-8.5379	3	1.9219	7	55001	304	4 0 4 3	3 0 3 4
38413.3361	0.0000	-6.7387	3	1.9219	7	55001	304	4 0 4 3	3 0 3 3
48012.7951	0.0000	-6.6448	3	3.2032	11	55001	304	5 0 5 5	4 0 4 5
48014.0962	0.0000	-5.3560	3	3.2032	9	55001	304	5 0 5 4	4 0 4 3
48014.1433	0.0000	-5.2646	3	3.2032	11	55001	304	5 0 5 5	4 0 4 4
48014.1641	0.0000	-5.1743	3	3.2032	13	55001	304	5 0 5 6	4 0 4 5
48014.4430	0.0000	-8.6403	3	3.2032	9	55001	304	5 0 5 4	4 0 4 5
48015.7912	0.0000	-6.6448	3	3.2032	9	55001	304	5 0 5 4	4 0 4 4
57615.0045	0.0000	-6.5693	3	4.8048	13	55001	304	6 0 6 6	5 0 5 6
57616.3435	0.0000	-5.1002	3	4.8048	11	55001	304	6 0 6 5	5 0 5 4
57616.3734	0.0000	-5.0252	3	4.8048	13	55001	304	6 0 6 6	5 0 5 5
57616.3886	0.0000	-4.9509	3	4.8048	15	55001	304	6 0 6 7	5 0 5 6
57616.6224	0.0000	-8.7245	3	4.8048	11	55001	304	6 0 6 5	5 0 5 6
57617.9913	0.0000	-6.5693	3	4.8048	11	55001	304	6 0 6 5	5 0 5 5
67216.8929	0.0000	-6.5067	3	6.7267	15	55001	304	7 0 7 7	6 0 6 7
67218.2563	0.0000	-4.8891	3	6.7267	13	55001	304	7 0 7 6	6 0 6 5
67218.2770	0.0000	-4.8255	3	6.7266	15	55001	304	7 0 7 7	6 0 6 6
67218.2887	0.0000	-4.7622	3	6.7267	17	55001	304	7 0 7 8	6 0 6 7
67218.4900	0.0000	-8.7966	3	6.7267	13	55001	304	7 0 7 6	6 0 6 7
67219.8742	0.0000	-6.5067	3	6.7266	13	55001	304	7 0 7 6	6 0 6 6
76818.4039	0.0000	-6.4537	3	8.9688	17	55001	304	8 0 8 8	7 0 7 8
76819.7845	0.0000	-4.7097	3	8.9688	15	55001	304	8 0 8 7	7 0 7 6
76819.7997	0.0000	-4.6544	3	8.9688	17	55001	304	8 0 8 8	7 0 7 7
76819.8089	0.0000	-4.5993	3	8.9688	19	55001	304	8 0 8 9	7 0 7 8
76819.9859	0.0000	-8.8601	3	8.9688	15	55001	304	8 0 8 7	7 0 7 8
76821.3816	0.0000	-6.4537	3	8.9688	15	55001	304	8 0 8 7	7 0 7 7
86419.4821	0.0000	-6.4083	3	11.5313	19	55001	304	9 0 9 9	8 0 8 9
86420.8754	0.0000	-4.5541	3	11.5313	17	55001	304	9 0 9 8	8 0 8 7
86420.8871	0.0000	-4.5052	3	11.5312	19	55001	304	9 0 9 9	8 0 8 8
86420.8945	0.0000	-4.4563	3	11.5313	21	55001	304	9 0 9 10	8 0 8 9
86421.0524	0.0000	-8.9173	3	11.5313	17	55001	304	9 0 9 8	8 0 8 9
86422.4574	0.0000	-6.4083	3	11.5312	17	55001	304	9 0 9 8	8 0 8 8
96020.0723	0.0000	-6.3689	3	14.4140	21	55001	304	10 01010	9 0 910
96021.4755	0.0000	-4.4172	3	14.4140	19	55001	304	10 010 9	9 0 9 8
96021.4847	0.0000	-4.3732	3	14.4139	21	55001	304	10 01010	9 0 9 9
96021.4908	0.0000	-4.3294	3	14.4140	23	55001	304	10 01011	9 0 910
96021.6334	0.0000	-8.9697	3	14.4140	19	55001	304	10 010 9	9 0 910

Frequency <sup>a</sup>	Uncertainty <sup>b</sup>	I <sup>c</sup>	D <sup>d</sup>	E <sub>lower</sub> <sup>e</sup>	g <sub>up</sub> <sup>f</sup>	Tag <sup>g</sup>	QnF <sup>h</sup>	Qn <sub>up</sub> <sup>i</sup>	Qn <sub>lower</sub> <sup>j</sup>
96023.0458	0.0000	-6.3689	3	14.4139	19	55001	304	10 010 9	9 0 9 9
105620.1196	0.0000	-6.3345	3	17.6169	23	55001	304	11 01111	10 01011
105621.5307	0.0000	-4.2952	3	17.6169	21	55001	304	11 01110	10 010 9
105621.5382	0.0000	-4.2553	3	17.6168	23	55001	304	11 01111	10 01010
105621.5433	0.0000	-4.2155	3	17.6169	25	55001	304	11 01112	10 01011
105621.6733	0.0000	-9.0183	3	17.6169	21	55001	304	11 01110	10 01011
105623.0918	0.0000	-6.3345	3	17.6168	21	55001	304	11 01110	10 01010
115219.5693	0.0000	-6.3044	3	21.1400	25	55001	304	12 01212	11 01112
115220.9869	0.0000	-4.1855	3	21.1400	23	55001	304	12 01211	11 01110
115220.9930	0.0000	-4.1491	3	21.1400	25	55001	304	12 01212	11 01111
115220.9974	0.0000	-4.1126	3	21.1400	27	55001	304	12 01213	11 01112
115221.1169	0.0000	-9.0639	3	21.1400	23	55001	304	12 01211	11 01112
115222.5406	0.0000	-6.3044	3	21.1400	23	55001	304	12 01211	11 01111
124818.3668	0.0000	-6.2780	3	24.9834	27	55001	304	13 01313	12 01213
124819.7898	0.0000	-4.0863	3	24.9834	25	55001	304	13 01312	12 01211
124819.7949	0.0000	-4.0527	3	24.9834	27	55001	304	13 01313	12 01212
124819.7987	0.0000	-4.0191	3	24.9834	29	55001	304	13 01314	12 01213
124819.9092	0.0000	-9.1072	3	24.9834	25	55001	304	13 01312	12 01213
124821.3373	0.0000	-6.2780	3	24.9834	25	55001	304	13 01312	12 01212
134416.4575	0.0000	-6.2548	3	29.1469	29	55001	304	14 01414	13 01314
134417.8850	0.0000	-3.9960	3	29.1469	27	55001	304	14 01413	13 01312
134417.8894	0.0000	-3.9648	3	29.1469	29	55001	304	14 01414	13 01313
134417.8927	0.0000	-3.9336	3	29.1469	31	55001	304	14 01415	13 01314
134417.9955	0.0000	-9.1485	3	29.1469	27	55001	304	14 01413	13 01314
134419.4274	0.0000	-6.2548	3	29.1469	27	55001	304	14 01413	13 01313
144013.7869	0.0000	-6.2346	3	33.6306	31	55001	304	15 01515	14 01415
144015.2183	0.0000	-3.9134	3	33.6306	29	55001	304	15 01514	14 01413
144015.2221	0.0000	-3.8843	3	33.6306	31	55001	304	15 01515	14 01414
144015.3211	0.0000	-9.1882	3	33.6306	29	55001	304	15 01514	14 01415
144016.7563	0.0000	-6.2346	3	33.6306	29	55001	304	15 01514	14 01414
153611.7352	0.0000	-3.8376	3	38.4345	31	55001	304	16 01615	15 01514
153613.2694	0.0000	-6.2169	3	38.4344	31	55001	304	16 01615	15 01515

<sup>1</sup> <sup>a</sup> Calculated frequency in MHz

<sup>b</sup> Calculated uncertainty of the line. If the line position is in units of MHz then uncertainty of the line is greater or equal to zero.

<sup>c</sup> Base 10 logarithm of the integrated intensity at 300K in nm<sup>2</sup> MHz

<sup>d</sup> Degrees of freedom in the rotational partition function (0 for atoms, 2 for linear molecules, 3 for non linear molecules)

<sup>e</sup> Lower state energy in cm<sup>-1</sup> relative to the lowest energy level in the ground vibronic state.

<sup>f</sup> Upper state degeneracy :  $g_{up} = g_I \times g_N$ , where  $g_I$  is the spin statistical weight and  $g_N = 2N + 1$  the rotational degeneracy.

<sup>g</sup> Molecule Tag

<sup>h</sup> Coding for the format of quantum numbers. QnF=100 × Q + 10 × H + N<sub>Qn</sub>; N<sub>Qn</sub> is the number of quantum numbers for each state; H indicates the number of half integer quantum numbers; Qmod5, the residual when Q is divided by 5, gives the number of principal quantum numbers (without the spin designating ones).

<sup>i</sup> Quantum numbers for the upper state

<sup>j</sup> Quantum numbers for the lower state